Superalloys 2012: 12th International Symposium on Superalloys
Edited by: Eric S. Huron, Roger C. Reed, Mark C. Hardy, Michael J. Mills, Rick E. Montero, Pedro D. Portella, Jack Telesman
TMS (The Minerals, Metals & Materials Society), 2012

GRAIN BOUNDARY DEFORMATION AND FRACTURE MECHANISMS IN DWELL FATIGUE CRACK GROWTH IN TURBINE DISK SUPERALLOY ME3

Jinesh Dahal[1], Kimberly Maciejewski[1], Hamouda Ghonem[1]
[1]Department of Mechanical Engineering, University of Rhode Island, Kingston, RI 02881, USA

Keywords: Nickel-based superalloy, Crack Growth, Transitional Frequency, Grain Boundary Sliding, Slip Band Spacing

Abstract

The objective of this paper is the development of a multi-scale, mechanistic based intergranular crack growth model, which considers creep, fatigue and environment interactions in a nickel disk material, ME3. In this model, the basic cracking mechanism involves grain boundary (GB) sliding and dynamic embrittlement, which are identified by examining the apparent activation energy, as well as, the slip/GB interactions in both air and vacuum environments. Modeling of the damage events is achieved by adapting a cohesive zone approach (an interface with internal singular surfaces) in which the GB dislocation network is smeared into a Newtonian fluid element. The deformation behavior of this element is controlled by the continuum in both far field (internal state variable model) and near field (crystal plasticity model) regions and the intrinsic GB viscosity which is able to define the mobility of the element by scaling up the motion of dislocations into a mesoscopic scale. This process is characterized by the rate at which the time-dependent sliding reaches a critical displacement and as such, a damage criterion is introduced by considering the GB mobility limit in the tangential direction leading to strain incompatibility and failure. Results of simulated intergranular crack growth rate, at different temperatures in both air and vacuum, are compared with those obtained experimentally. The model sensitivity is examined by performing case studies of materials with varying GB viscosity and different partial pressures of oxygen.

Introduction

This work focuses on the steady-state cracking process in a powder metallurgy (P/M) nickel-based superalloy at elevated temperatures. In general, the cracking mechanisms in these types of alloys are described by two distinct processes; cycle-dependent and time-dependent damage processes. The cycle-dependent cracking takes place along slip planes and occurs at frequencies higher than the material's transitional frequency, which is a function of the load ratio, temperature, environment and intrinsic factors of the microstructure [1-3]. On the other hand, time-dependent crack growth, achieved at loading frequencies below the transitional frequency, is a thermally activated process which is characterized by intergranular cracking [4-6]. Typical applications of nickel based superalloys, particularly aero engines, include hold times at elevated temperature, thus promoting intergranular fracture. The mechanisms associated with this fracture mode involve creep and environment related damage processes. The creep damage is described by cavitation and/or GB sliding, while environment is viewed as either stress assisted grain boundary oxidation or dynamic embrittlement processes.

The first part of this study, identifies the GB cracking mechansims in ME3 as GB sliding and dynamic embrittlement processes in the temperature range 650°C-800°C. These mechanisms are implemented in a cohesive zone model in which the continuum material is described by multi-scale constitutive equations. Furthermore, the GB sliding process is governed by the stress field present at the GB crack tip, which controls the slip/GB interactions. The high stress at the crack tip causes dissociation of lattice dislocations, present in a slip band, into a sessile dislocation and a mobile glissile dislocation, thus inducing GB sliding. In addition, the stress drives the oxygen from the environment which embrittles the GB. The interaction of creep and environment is considered through a fracture criterion in which the GB sliding limit is reduced by the GB mobility due to dynamic embrittlement. The validity of the cohesive zone model is determined by comparing the simulated and experimental crack growth rates at the temperatures mentioned above.

Time-Dependent Crack Growth Rate

The material in this study, ME3, is heat treated at super-solvus conditions, resulting in a planar grain boundary with an average grain size of 44 μm (ASTM 6) and a bimodal size distribution of γ' precipitates. The larger particles, secondary γ' (γ'_s), appear cubical (see Fig. 1a), while the smaller ones, tertiary γ' (γ'_t), are spherical (see Fig. 1b). Sizes and volume fractions of the γ'_s are 230 nm and 41%, respectively, while for γ'_t, the measurements are 42 nm and 10%, respectively, where the precipitate sizes are reported as the equivalent particle diameter.

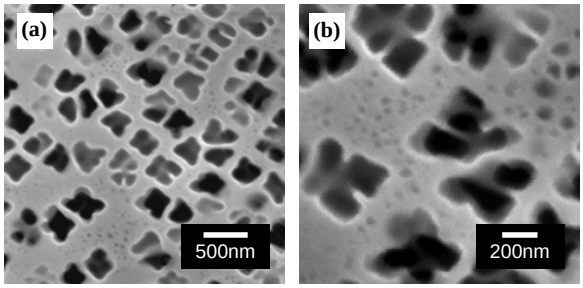

Figure 1: Secondary electron image of the as received ME3 microstructure, etched with AG-21 for 15sec, showing (a) γ'_s size and distribution and (b) γ'_t particles within the matrix.

Dwell-fatigue crack growth tests were performed on standard compact tension (CT) specimens with dimensions following ASTM E647, using servohydraulic fatigue testing machines with the crack growth measurements being monitored using the potential drop technique. Pre-cracking was first performed at room temperature between 5-10 Hz. The loading cycle, during the test, consists of 1.5s loading, 1.5s unloading and a dwell time of 0s, 30s, 100s, 300, 600, 3000 and 7200s superimposed at the maximum load level with an initial starting ΔK in the range of 28-32 MPa√m. All tests were performed at a stress ratio of 0.1 at three temperature levels; 650, 704 and 760°C in an air and

vacuum environments. For each vacuum test, the vacuum pressure is maintained in the range of 10^{-6} to 10^{-7} torr during the entire test. Results of these tests in terms of da/dN versus ΔK, as shown in Fig. 2, show that the crack growth rate increases with both temperature and hold time duration.

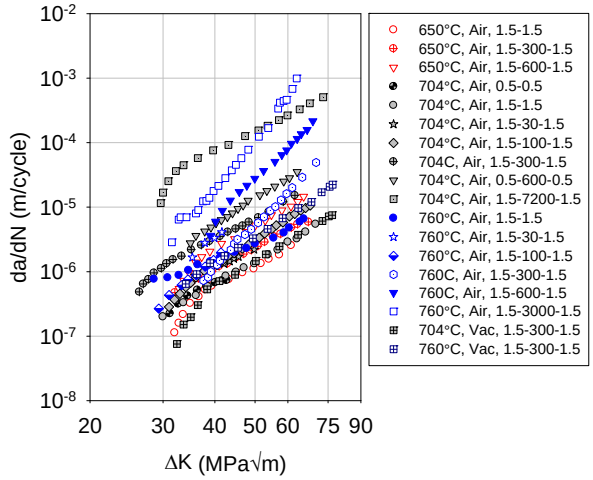

Figure 2: da/dN versus ΔK at 650, 704 and 760°C for various loading frequencies in both air and vacuum environments.

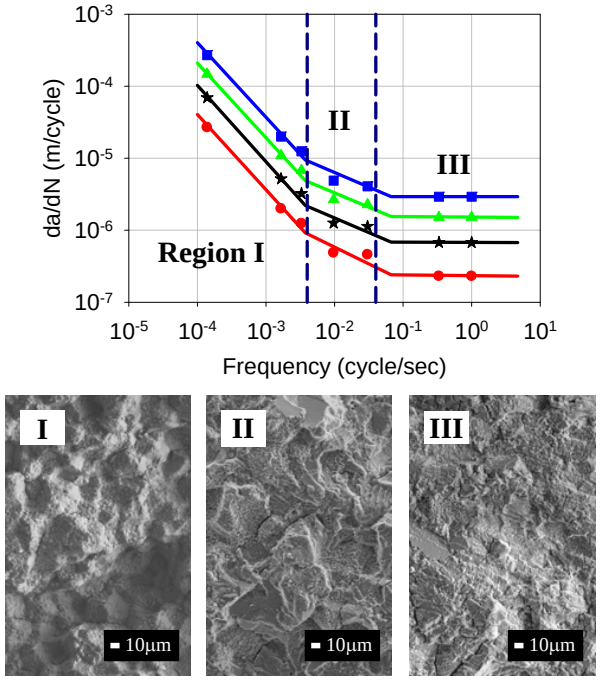

Figure 3: Typical da/dN versus frequency curves for various values of ΔK at 704°C and typical intergranular, mixed mode, and transgranular fracture surfaces corresponding to regions I, II and III; respectively.

The frequency effects are examined in terms of cycle-dependent and time-dependent damage mechanisms by plotting da/dN versus frequency, *f*, and examining the corresponding fracture modes, as shown in Fig. 3. This figure shows that the transition between transgranular and intergranular fracture modes is defined by a transitional frequency, f_t, which is found to be approximately 0.01 Hz for the three test temperatures. Region I ($f < f_t$) is low frequency associated with an intergranular fracture. In addition to air environment, intergranular fracture has been observed in a vacuum environment for a loading cycle of 1s-300s-1s, at both 704°C and 760°C. Region II ($f \sim f_t$) is an intermediate frequency region associated with a mixed transgranular/intergranular fracture mode. Region III ($f > f_t$) is high frequency, associated with a transgranular fracture mode. These loading conditions are cycle-dependent in nature, which is indicated by the lack of dependency between da/dN and *f* in Region III. The intergranular crack growth curves, in terms of da/dt versus K_{max}, are shown in Fig. 4.

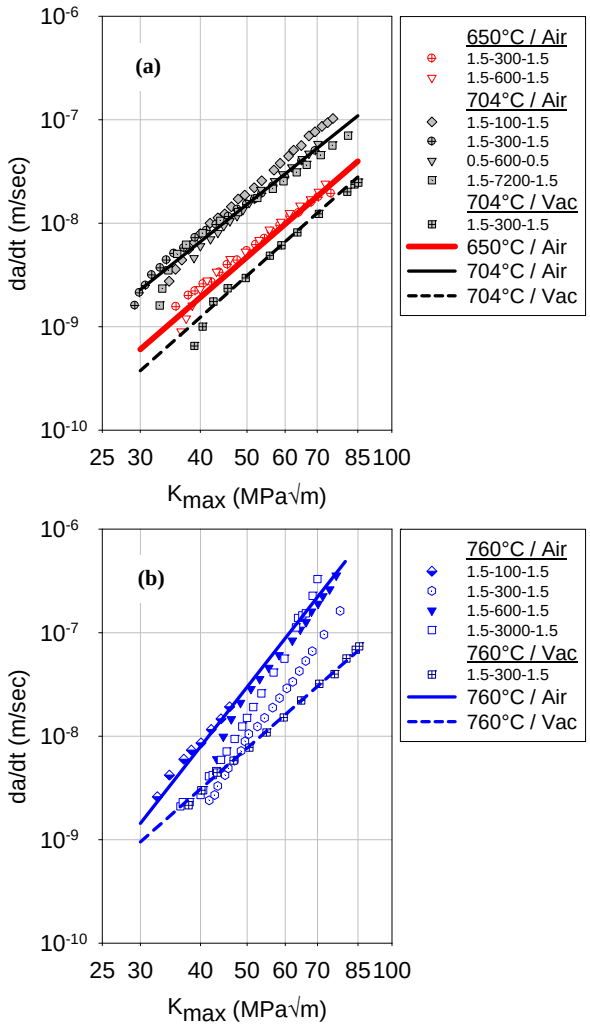

Figure 4: Crack growth rate in terms of da/dt versus K_{max} in air and vacuum environments at (a) 650°C, 704°C and (b) 760°C.

This figure shows that the crack speed is temperature dependent. Furthermore, for each of the test temperatures, the crack growth curves consolidate into a single line pointing out to the fact that da/dt for the same K_{max} is independent of the length of the hold time. This result indicates that the crack growth process is continuous in nature and does not involve damage events that require an incubation time. As will be detailed later in the paper, this conclusion precludes the presence of dynamic embrittlement by oxygen diffusion as an active damage mechanism. Fig. 4b, shows that the consolidation of the crack speed at 760°C for different hold time is not complete. This behavior may be due to other damage mechanisms operating at this temperature, that do not exist at 650°C or 704°C. One possibility is that the microstructure is unstable at 760°C, since this is the aging temperature of the ME3 alloy which, combined with high stresses, could result in dissolution of the tertiary γ' particles in the immediate crack tip region, see Fig. 5.

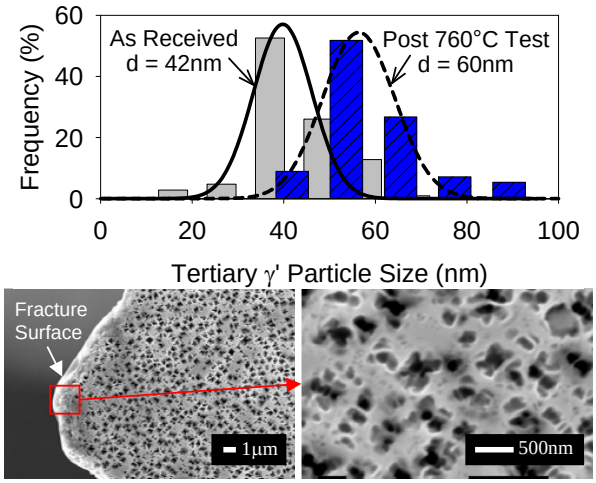

Figure 5: Secondary electron image of an etched ME3 specimen post-testing at 760°C in an air environment revealing dissolution of the tertiary γ'precipitates near the crack tip, where the average size is larger than that of the as received material as shown by the γ' particle distributions.

The tertiary γ' particle sizes are measured in a grain which is located directly adjacent to the crack path. Fig. 5 indicates that the tertiary γ' particle distribution has shifted its mean size from 42 nm to 60 nm after testing at 760°C. This implies that there is coarsening and dissolution of the tertiary γ' precipitates at the crack tip. This possible damage mechanism will not be considered in this paper and analysis of the crack growth process at 760°C, presented in the next section, will only consider the average position of the scattered region shown in Fig. 4b, which represents the typical behavior of ME3 at 760°C in air.

Intergranular Cracking Mechanisms

Identifying the cracking mechanisms in time-dependent fracture processes can be achieved by examining the corresponding apparent activation energy, *Q*. Since the cracking process is thermally activated, *Q*, can be determined from results in Fig. 4. The calculated values of the apparent activation energy in both air and vacuum environment are plotted versus K_{max} in Fig. 6. In this figure, the *Q* versus K_{max} relationship can be fit into a polynomial equation of the form:

$$Q = Q_0 + Q_a\left(K_{max}\right) + Q_b\left(K_{max}\right)^2 \quad (1)$$

where *Q* is in kJ/mol and the three constants Q_0, Q_a, and Q_b are 224.2, -1.6, and 7.39E-3 in air and 144.1, -0.2 and 0 in vacuum; respectively.

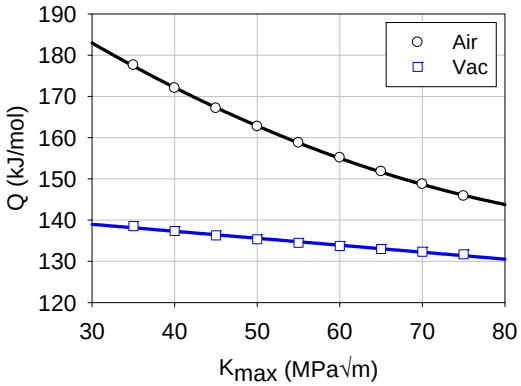

Figure 6: Apparent activation energy as a function of K_{max} in an air and vacuum environment.

The results show that for K_{max} between 30 and 80 MPa√m , *Q* in vacuum is lower than that in air, with air values ranging from 140-180 kJ/mol, while for vacuum it is in the range of 130-140 kJ/mol. The variations in apparent activation energy have two extreme cases for failure; thermal and athermal failure [7]. The former mode of failure occurs when the thermal energy, in the absence of stress, is sufficient to cause failure. The stress free energy, in this case, can be calculated by setting K_{max} to zero in equation (1), thus yielding $Q = Q_0$. On the other hand, athermal failure occurs when the stress, in the absence of thermal activation, is sufficient to cause failure. This failure mode could occur as a single or a multiple mechanism process. An approach to identify the nature of this process is by examining the value of *Q* corresponding to the asymptote $dQ/dK_{max} = 0$. For a single athermal process, K_{max} approaches infinity or a threshold value (K_{max}^{ath}) at which $Q = dQ/dK_{max} = 0$. On the other hand, a multiple damage process would correspond to a condition where at $dQ/dK_{max} = 0$, the value of $Q(K_{max}^{ath})$ approaches a finite value [8]. The athermal threshold stress, K_{max}^{ath}, is determined by equating the derivative of equation (1) with respect to K_{max}, to zero which yields a value of 108 MPa√m in air at which the activation energy is a finite value of 138 kJ/mol indicating the presence of multiple damage processes. In vacuum, since *Q* is idealized as a linear function of K_{max}, K_{max}^{ath} is taken to be equal to that at $Q = 0$ which in turn identifies a single fracture process operating at the crack tip. The nature of the operating damage process is determined by comparing the current results of *Q* for ME3 to those identified in relation to known mechanisms by Starink and Reed [9]. The activation energy in vacuum in the range of 130-140 kJ/mol, corresponds to a single damage mechanism involving grain boundary (GB) creep. On the other hand, the values of *Q* in air are in the range of 140-180 kJ/mol which identifies a multi damage mechanism involving GB creep enhanced by oxidation processes. The environmental damage process in this alloy has been mainly

attributed to dynamic embrittlement associated with oxygen diffusion. This is supported by the experimental observations that the da/dt is hold time independent at a constant temperature, and the crack length, as well as, the crack opening displacement as a function of number of cycles, are continuous in nature. This suggests, as mentioned earlier, that the cracking process does not involve damage events that require incubation time and that environmental damage due to oxide formation can be precluded as a possible damage mechanism. Furthermore, creep damage could be attributed to cavitation and/or GB sliding. Examination of fracture surfaces have shown no evidence of cavities in this alloy, thus, the sliding mechanism is considered to be dominant. The GB sliding in ME3 specimens has been observed using a pre-test scribing method, in which surface measurements of GB sliding post-testing are taken as the amount of shift in the scribe line in the direction parallel to the GB cracking path. This average measurement is calculated in the range of 1 to 6 microns. Typical micrographs showing the shift in scribe lines, i.e. GB sliding, are shown in Fig. 7 for tests in both air and vacuum.

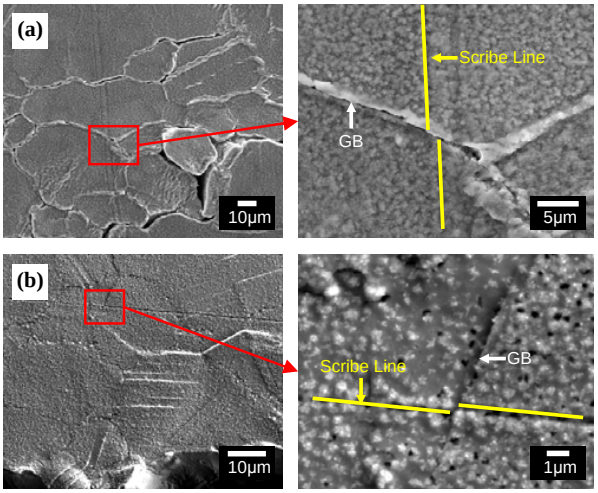

Figure 7: Post-test grain boundary sliding observations in hold time tests at 760°C in an (a) air and (b) a vacuum environment.

Intergranular Crack Growth Model

This section describes the main features of a cohesive zone (CZ) model that has been developed to simulate intergranular cracking in the ME3 alloy at elevated temperatures. This model is built using a multi-scale approach which utilizes the knowledge of the GB external and internal deformation fields. The external field is generated by developing and coupling two continuum constitutive models including (i) a macroscopic internal state variable model for the purpose of modeling the response of the far field region located several grains away from the crack path and (ii) a near field, microstructure explicit coarse scale crystal plasticity model in which the isotropic and kinematic hardening parameters are explicitly dependent on γ' precipitate size and volume fraction. This scale is appropriate for the representation of the continuum region at the immediate crack tip. The second requirement in the implementation of the CZ model is a GB deformation model which has been developed on the basis of viscous flow rules of the boundary material. These rules correlate the rate of the GB sliding displacement to material and load dependent parameters. A damage criterion is introduced as a critical sliding limit which is degraded by the effects of oxygen diffusion leading to failure along the GB. The basic components of this CZ model is described below.

Continuum Material: Two regions are mathematically modeled here, the location of each, far field and near field, is described with respect to the crack tip interface. The far field region represents the continuum at several grains distance from the grain boundary fracture path. It is described by an internal state variable (ISV) constitutive model based on non linear kinematic hardening laws. The near field region, which is comprised of several grains in direct contact with the GB fracture path, is described by a coarse scale crystal plasticity model (XP), following the classical finite deformation theory, considering hardening of the 12 slip systems of the FCC crystal. This region consists of an array of 100 grains, each with an orientation within ±15° of its neighboring grains. Both scale models consider isotropic and kinematic hardening components, in which a two term back stress variable includes the effects of dynamic and static recovery. The material parameters for the ISV and XP models are obtained from results of a wide range of low cycle fatigue tests which were performed at three temperatures, 650, 704 and 760°C, at different strain rate and strain range conditions. Details of these models are given elsewhere [4].

GB Interface: The GB interface is modeled using a CZ approach in which the GB dislocation network is smeared into a Newtonian fluid element. The interface is considered to be a node-to-node contact and is described by traction-displacement laws. These laws follow a viscoelastic relationship in which the tangential elastic opening displacement is the difference between the total and GB sliding displacements. The traction-displacement laws acting on the GB phase can be described as:

$$T_n = k_n\left(u_n - u_c\right) \tag{2}$$

$$T_t = k_t\left(u_t - u_s\right) \tag{3}$$

where the subscripts n and t represent normal and tangential directions, respectively, $T_{n,t}$ is the GB traction, $k_{n,t}$ is the cohesive stiffness, $u_{n,t}$ is the total opening displacement, u_c is the normal opening displacement due to cavities and u_s is the tangential displacement due to GB sliding. In the current analysis, u_c = 0, due to the absence of cavity related deformation mechanisms. The GB sliding is described by a viscous flow law which is written as the relative velocity of two sliding layers [10]:

$$\dot{u}_s = \left(\delta/\eta\right)T_t \tag{4}$$

where δ is the GB thickness, η is a proportionality factor (GB viscosity term) and T_t is the tangential stress. The viscosity term can be derived following the approach of Kê [11], where the rate of relative displacements of the sliding surfaces can be described by the distance slipped along the GB during the relaxation time, t_c which is the time required by a dislocation to climb a distance λ at a velocity, v_c. This velocity is given by the Einstein mobility relation as the product of the mobility of GB dislocations, M_d, and the force per unit length acting on the dislocation [12-14]. This approach yields the expression:

$$\eta = \left(\delta E_{GB}/w_c\right)t_c = \left(\delta E_{GB}/w_c\right)\left(\lambda/M_d T_t b\right) \quad (5)$$

where E_{GB} is the unrelaxed shear modulus, w_c is the characteristic length over which GB sliding occurs and b is the Burger's vector. The intrinsic mobility term, M_d, is a function of the GB diffusivity, D_{gb}, Boltzmann's constant, k, and temperature, T, and is expressed as:

$$M_d = D_{gb}/kT \quad (6)$$

Substituting equation (5) into (4) yields the sliding rate in terms of dislocation mobility, given as:

$$\dot{u}_s = w_c\left(M_d b/E_{GB}\lambda\right)T_t^2 \quad (7)$$

The GB sliding strain rate is obtained by dividing equation (7) by the characteristic length w_c. This rate is written as:

$$\dot{\varepsilon}_s = \dot{u}_s/w_c = \left(M_d b/E_{GB}\lambda\right)T_t^2 \quad (8)$$

Slip/GB Interactions: The sliding rate described in equations (7) and (8) are a function of the critical sliding length, w_c which is the minimum length required between two pinning points over which GB sliding occurs. This length has been experimentally determined by analyzing the interactions between lattice dislocations within the slip band and the GB. The macroscopic strain, during cyclic loading, is distributed either homogenously or heterogeneously along a collection of slip bands [15,16]. The plastic deformation is concentrated locally along these bands, which generally extends between two grain boundaries. The optimum number and spacing of slip bands is based on a minimum energy configuration which indicates the absence of long range stresses in the bulk [17]. A model of slip band spacing as a function of loading parameters is formulated on the basis of a criterion of minimum strain energy accumulation within slip bands and that a unique configuration of number and spacing of bands exists for a given plastic strain [16]. Based on previous work [5], the slip band spacing as a function of global loading parameters is give as:

$$w^2 = \frac{(1-\nu)ah}{2M^2GB}\frac{\left(\Delta\sigma - 2\sigma_F\right)}{\varepsilon_p \exp\left(B' f\right)} \quad (9)$$

where w is slip band spacing, ν is Poisson's ratio, a is the pile-up length, h is the width of a slip band, M is the Taylor factor, G is shear modulus, f is the loading frequency, ε_p is the applied tensile plastic strain, $\Delta\sigma$ is the remote tensile stress, σ_F is the frictional stress, B and B' are material constants. The resulting curve, shown in Fig. 8, has been optimized by experimental measurements of slip band spacing for a high and low frequency loading. Fig. 8a shows three regions which are similar to those described previously. The transition between transgranular and intergranular fracture modes in Fig. 3 and 8a can be interpreted in terms of slip line density or spacing resulting in compatibility or incompatibility along the GB [5]. The incompatibility results in a

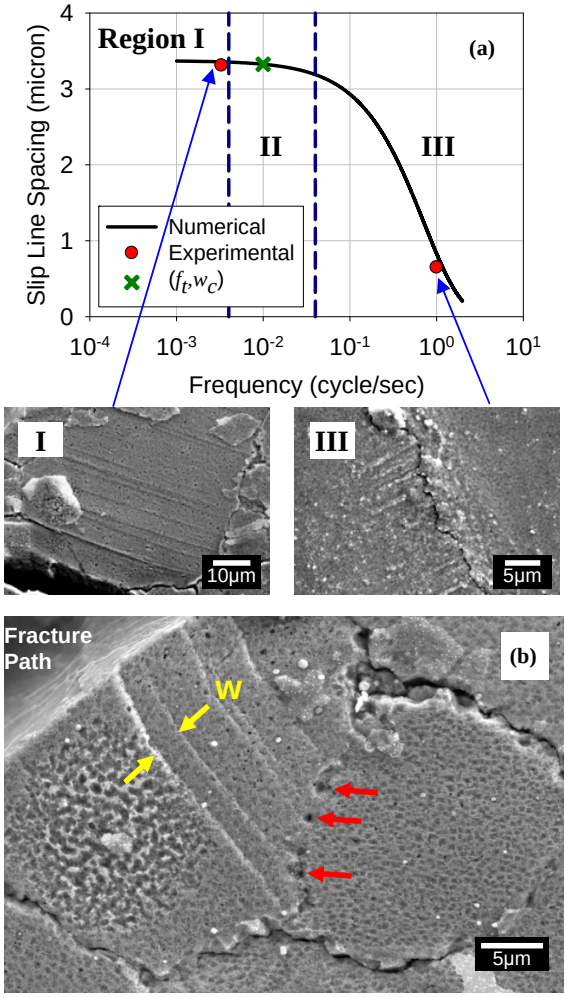

Figure 8: (a) Slip band spacing as a function of loading frequency at 760°C, with secondary electron micrographs of unetched specimens, post-testing, showing large and small slip band spacing corresponding to region I and III; respectively. (b) Secondary electron micrograph showing surface GB openings (red arrows) during a dwell fatigue crack growth test at 760°C in a vacuum environment indicating that GB sliding is limited to lengths between slip bands (w).

stress concentration, which is responsible for intergranular fracture. During high loading frequency, there is a small slip band spacing (high slip band density) resulting in compatibility along the GB allowing slip transmission in which there is no stress build up along the GB, therefore failure is by fatigue along the slip plane (transgranular fracture). On the other hand, during low loading frequency, where there is a large slip band spacing (low slip band density), an incompatibility along the GB results in no transmission of dislocations across the GB. As a result, a stress concentration is built up at the GB causing the lattice dislocation to dissociate into two extrinsic GB dislocations [18-22]; one parallel to the GB plane and the other perpendicular to it. Failure then occurs when the glissile dislocations present in the GB glide [20], i.e. local GB sliding, until reaching an obstruction, resulting

in intergranular fracture. With fewer slip bands, the obstruction of sessile dislocations is reduced and the available sliding distance (which is the slip band spacing) is higher. In Fig. 8a, the critical slip band spacing, above which GB sliding occurs (intergranular fracture), corresponds to the spacing measured at the transitional frequency, $w(f_t)$, taken as approximately 3 microns. This critical value of slip band spacing, w_c, represents a minimum length for mobility of the gliding GB dislocations in order to create an incompatibility between the two relative grains resulting in GB sliding. The limit of the GB length over which sliding would occur could be as long as the grain size which would provide a crack growth pattern in a discrete step-wise form. However, it is observed from crack opening displacement measurements, that the crack growth is a continuous process. This is also supported by the general observation that the GB openings are limited to lengths smaller than the grain size, as shown in Fig. 8b.

GB Fracture Criterion: As discussed earlier, intergranular cracking, in the ME3 alloy in the temperature range studied, occurs by coupled GB sliding and dynamic embrittlement. It has been shown that intergranular fracture occurs in both air and vacuum environments, thus, a fracture criterion is considered here to be a critical GB sliding limit modified by environment. The accelerated damage in the crack tip GB path in air environment is considered to be a result of GB dynamic embrittlement by oxygen diffusion, the effect of which is to pin the GB dislocations and reduce their effective mobility. Fracture occurs once the accumulated oxygen at the crack tip is sufficient to result in GB immobility leading to a localized boundary decohesion. This embrittlement mechanism is the basis of a GB fracture criterion formulated in terms of the critical sliding strain in vacuum reduced by a GB mobility parameter which is a function of the oxygen concentration [5]. This critical strain is written as:

$$\varepsilon_{crit} = \varepsilon_{crit0} - z/M_{O2} \tag{10}$$

where ε_{crit0} is the critical strain for GB sliding in vacuum obtained as a function of temperature. This strain limit is degraded by the factor z/M_{O2}, where z is a temperature dependent, oxygen diffusion related constant. The dislocation mobility in the presence of impurity atoms, M_{O2}, decreases due to the drag caused by segregated impurities [12, 13] and is a function of diffusivity of oxygen in the GB, D_{O2}, and oxygen concentration in the bulk material, C_{O2}. The D_{O2} is expressed by an Arrhenius type of law and C_{O2} can be derived from Fick's first and second law. The mobility, diffusivity and concentration terms are described by:

$$M_{O2} = \frac{D_{O2}\Omega}{kTb^2 C_{O2}} \tag{11}$$

$$D_{O_2} = D_0 e^{-Q_{O_2}/RT} \tag{12}$$

$$C_{O_2} = C_0 + (C_S - C_0)\left[1 - erf\left(r/2\sqrt{D_{O_2} t}\right)\right] \tag{13}$$

where Ω is the atomic volume, D_0 is the frequency factor, Q_{O2} is the stress dependent activation energy for diffusion of oxygen in the GB, R is the universal gas constant, T is absolute temperature, C_0 is the initial concentration of oxygen in the bulk material, C_S is the concentration of oxygen in air, r is the distance from the crack tip and t is time. This criterion in combination with the model described above are utilized to simulate the intergranular crack growth process due to GB sliding and dynamic embrittlement.

Intergranular Crack Growth Rate Simulations

Validation of the CZ model described above has been carried out by comparing the simulated crack growth data with that obtained experimentally. This comparison is used to optimize the different model components which determine the sliding displacement and concentration of oxygen at the crack tip. Additionally, this provides a route to assess the relative significance of each of these components to the intergranular damage associated with dwell fatigue crack growth in the ME3 alloy. For this purpose, case studies were performed in order to illustrate the sensitivity of the CZ model to variations in intrinsic GB mobility, as well as, different oxygen partial pressure conditions within the range of temperatures utilized in this study.

Influence of Temperature and Environment (650°C-800°C)

Case studies performed at temperatures of 650, 704 and 760°C under sustained loading conditions (i.e. a loading time of 1.5s then constant load), at different K_{max} values, are presented in this section.

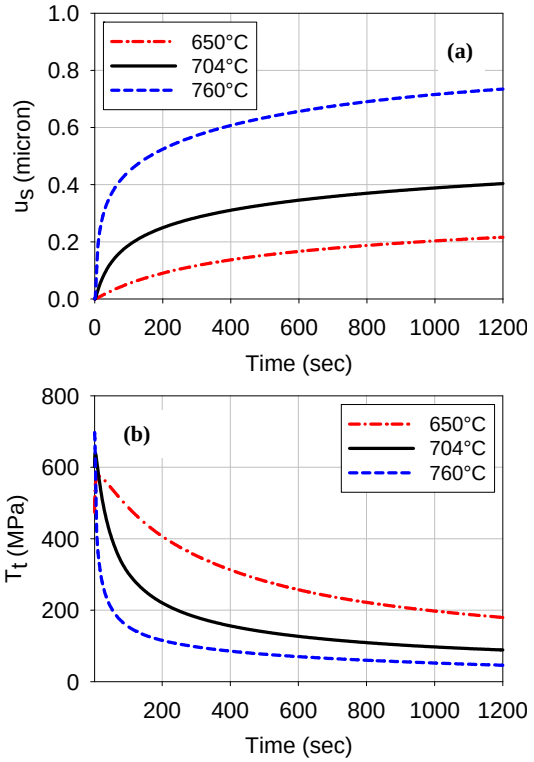

Figure 9: (a) GB sliding displacement and (b) tangential traction across the grain boundary as a function of time and temperature at a K_{max} of 55 MPa√m under sustained load crack growth conditions.

Fig. 9a illustrates that the sliding displacement as a function of time shows a rapid increase followed by saturation. In addition, this displacement increases rapidly with the increase in temperature. At 1000 seconds, the sliding displacement at 704 and 760°C are 2 and 3.5 times higher respectively than that at 650°C. This behavior can be attributed to the rapid relaxation in the tangential traction with the increase in temperature, as seen in Fig. 9b. Initially, the tangential traction is higher at 760°C, but the rapid decline in traction is enhanced by the large sliding displacement. As the sliding displacement becomes comparable in value to the total tangential displacement, the elastic component vanishes and the tangential traction approaches zero as time increases.

Results obtained from the simulation of crack growth without environment effects are validated by comparing with the crack growth experiments performed in vacuum. The effect of environment is nullified by putting the concentration of oxygen at the surface (C_s) equal to zero and the fracture limit is defined solely by ε_{crit0}. Fig. 10a shows the simulated curves compared with crack growth experiments in vacuum. The numerical crack growth curves for 704°C and 760°C in vacuum are shown to follow a trend similar to that of the experimental data. The slopes of the simulated set expressing a relatively higher power. The simulated data show under prediction of the crack growth rates at lower K_{max} values, while the opposite is observed at high K_{max}. This is possibly due to the stress sensitivity of the GB sliding rate to the stress exponent which is used in the calculation of GB sliding displacement. In addition to the 650-760°C temperature range, the crack growth process was also examined at 800°C in an air environment. The experimental crack growth rate at this temperature is similar to that at 760°C. The crack growth rates for temperatures ranging from 650 to 800°C in air environment have been predicted and the results are shown in Fig. 10b and 10c. The numerical results of the four temperatures studied are in agreement with the range and trends of the experimental crack growth data. Similar to the vacuum results, the numerically simulated crack growth rate curves in air can be represented by a power law form. However, in contrast to vacuum results, air simulated curves show a slope slightly lower than that obtained in the experimental curves. This is due to the difficulty in determining the frequency term of the oxygen diffusivity function. The low K_{max} region can be identified as a more temperature dependent region, with an increased effect of environment. The impact of both temperature and environment reduces in the upper crack growth region. The discussion of low da/dt and low K_{max} region in the presence of environment is described as a stress independent region where oxygen embrittlement occurs as more time for diffusion of oxygen in the GB is available which results in higher crack growth rates [23, 24].

Influence of Oxygen Partial Pressure

The partial pressure of oxygen has been studied by varying the surface concentration of oxygen, C_s, from vacuum conditions (C_s = 0%) to that of an air environment (C_s = 21%). The difference between the surface concentration of oxygen and the concentration of oxygen in the bulk material, C_s - C_0, controls the oxygen flux and its reduction decreases the diffusion of oxygen in the GB. The concentration of oxygen in the GB controls the critical sliding strain which is calculated as a function of the GB mobility, M_{O2}, and is proportional to T and C_{O2}, given in equations (10) to (13). The effect of C_s on the critical sliding strain at a K_{max} of 55 MPa√m is shown in Fig. 11. This figure illustrates that the time to fail, i.e. the intersection of the critical sliding strain with the developed GB sliding strain, increases with the reduction of both temperature and surface concentration of oxygen. It is interesting, however, to observe that the influence of C_s on the critical sliding strain is relatively higher at 650°C than the other two higher temperatures.

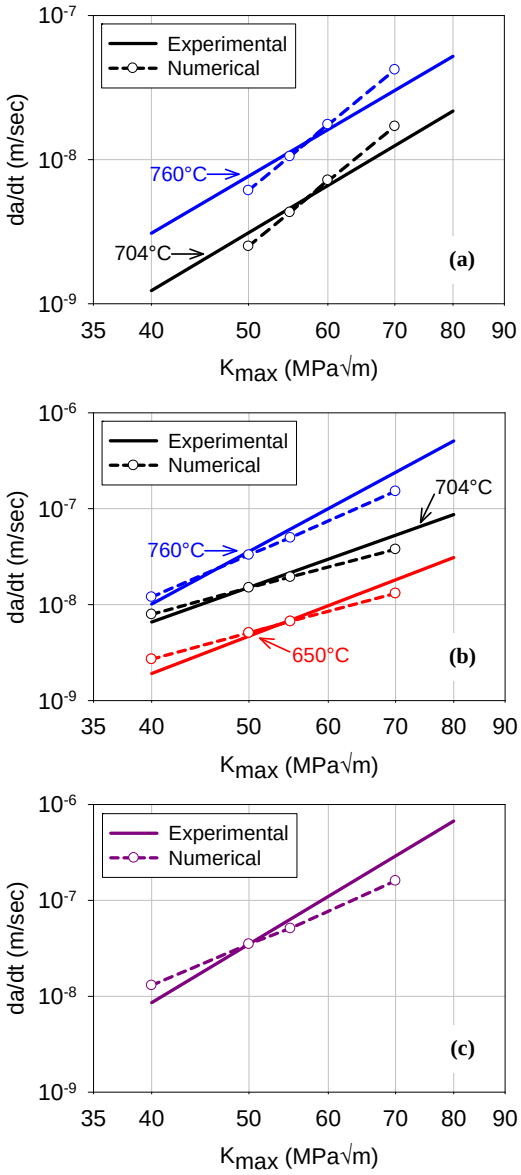

Figure 10: Experimental and numerical crack growth rate as a function of K_{max} at (a) 704 and 760°C in vacuum environment, (b) 650, 704 and 760°C in air environment and (c) at 800°C in air.

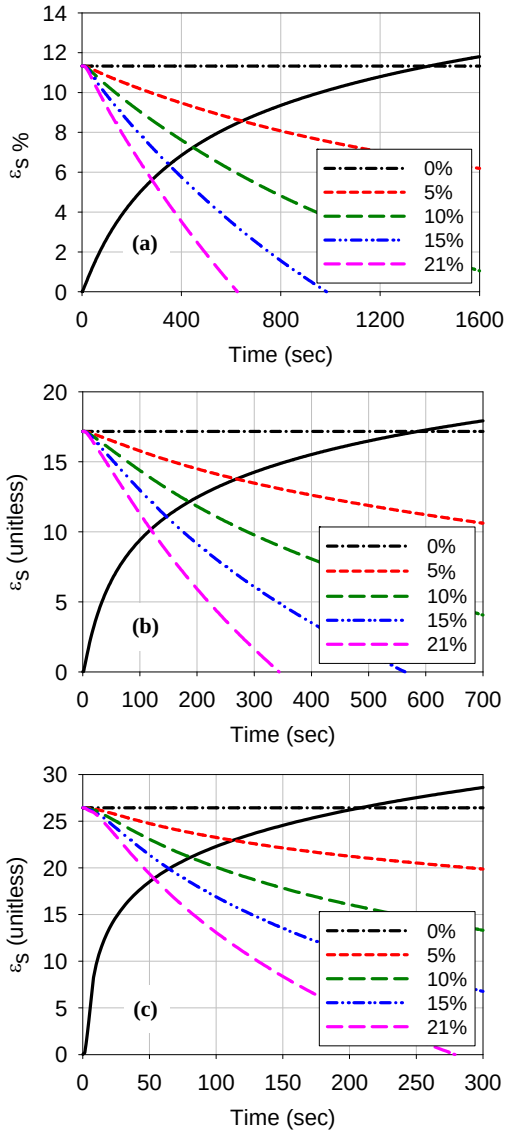

Figure 11: Grain boundary sliding strain (solid black line) as a function of time for (a) 650, (b) 704 and (c) 760°C under sustained load crack growth conditions at a K_{max} of 55 MPa√m. The dotted lines indicate the critical sliding strain as a function of time for environments varying from air (C_s = 21%) to vacuum (C_s = 0%).

Influence of GB Viscosity (GB Diffusivity and GB Modulus)

The role of GB viscosity, η, is presented here by modifying either the GB diffusivity, D_{gb}, or GB modulus, i.e. the unrelaxed shear modulus, E_{gb}. By decreasing D_{gb}, the intrinsic dislocation mobility, described by equation (5) is lowered. In turn, this would increase the η and increase the resistance of the GB to sliding. Increasing the stiffness of the GB, described by E_{gb}, would also increase η. By decreasing the D_{gb} by 50% or increasing the E_{gb}, by a factor of 2, the GB viscosity is changed by a factor of 2, from η_1 to $2\eta_1$. This increase in η, is shown in Fig. 12 to reduce the sliding rate and sliding displacement. This reduction would result in a decrease in crack growth rate. The decrease of u_s is high at higher K_{max} loading conditions compared to the observed decrease at lower K_{max} loading conditions for all temperatures. This non linear stress dependency of sliding causes a higher crack growth rate decrease at higher stresses, i.e. the difference in crack growth rate from 35 to 45 MPa√m is lower than that from 65 to 75 MPa√m.

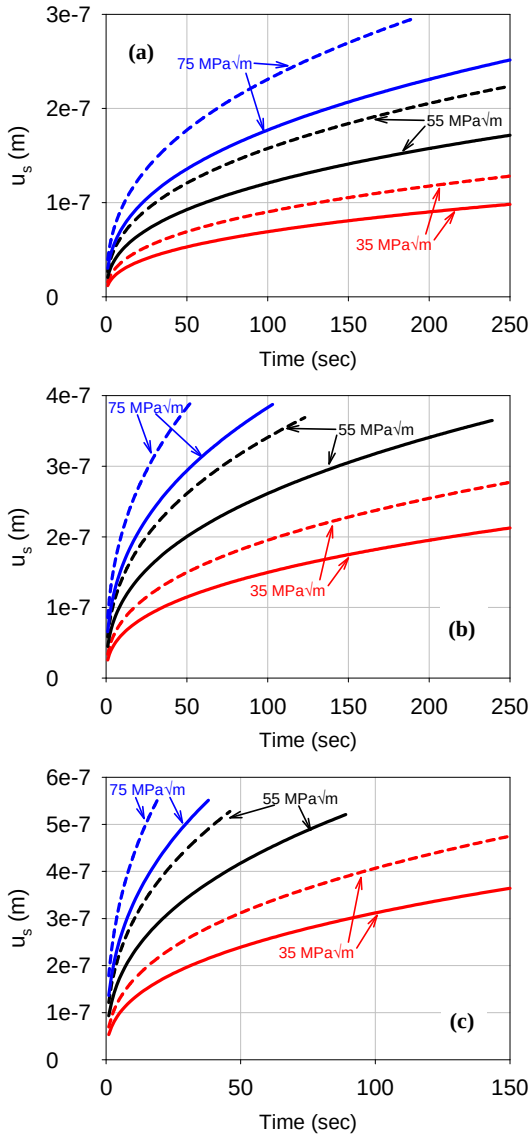

Figure 12: Grain boundary sliding displacement as a function of time and K_{max} for two GB viscosities, η_1 (dashed line) and $2\eta_1$ (solid line), at (a) 650, (b) 704 and (c) 760°C under sustained load crack growth conditions [5].

Summary and Conclusions

In this work, a mechanistic based time-dependent crack growth model, considering the role of creep and environment has been developed for the nickel-based alloy, ME3. To achieve this, combined experimental, analytical and numerical studies have been performed on ME3 alloy. In the experimental work, crack growth tests were carried out at four temperatures, 650, 704, 760 and 800°C, in both air and vacuum environment. Results of these tests are presented in the form of da/dN versus ΔK. A fracture surface analysis was conducted for each test condition and the fracture mode was identified as a function of loading frequency and temperature. This analysis provided the data input required to determine the transgranular/intergranular transitional frequency (f_t). Furthermore, the apparent activation energy (Q) was calculated from the slope of the crack growth rate as a function of temperature. Resulting values of Q have been used to determine basic damage processes involved in the intergranular cracking mechanisms in ME3 alloy. These have been identified as GB sliding coupled with dynamic embrittlement due to oxygen diffusion. The GB sliding mechanism was correlated with slip band/GB interactions and the ensuing dissociation of lattice dislocations resulting in the presence of mobile GB glissile dislocations leading to GB sliding. A criterion of this mechanism is that the slip band spacing (inverse of slip band density) exceeds a characteristic length, w_c. Analytical work has been developed to correlate the slip band spacing and loading frequency on the basis of minimum strain energy accumulation within a slip band. Results of this experimental/analytical work represent the input parameters necessary for implementation and validation of a mechanistic based time-dependent crack growth model which considers the role of creep, fatigue and environment interactions on both the bulk and the grain boundary interface in the ME3 disk material. The model has been established by considering a moving crack tip along a GB path in which damage events are described in terms of the GB deformation and related accommodation processes. Modeling of these events is achieved by adapting a CZ approach in which the GB dislocation network is smeared into a Newtonian fluid element. The deformation behavior of this element is controlled by the continuum in both far field (ISV model) and near field (XP model) and the intrinsic GB viscosity. The GB cracking process is controlled by the rate at which the time-dependent sliding reaches a critical displacement and as such, a damage criterion is introduced by considering the mobility limit in the tangential direction leading to strain incompatibility and failure. This limit is diminished by environmental effects which are introduced as a dynamic embrittlement process that hinders grain boundary mobility due to oxygen diffusion. The outputs of the numerical analysis are compared with those experimentally obtained and are used to identify the sensitivity of the crack growth to variations in GB viscosity and oxygen partial pressure. The main conclusions of this study are summarized as follows:

- A transgranular/intergranular transtitional frequency, f_t, has been identified as 0.01 Hz. For loading frequencies less then f_t, the crack speed, da/dt, was shown to be temperature dependent, but independent of hold time.
- The apparent activation energy, Q, for the intergranular cracking mechanism has been measured in the range of 130-140 kJ/mole in vacuum reaching 140-180 kJ/mole in air environment. Q is correlated in a non linear form with K_{max}, the analysis of which classifies that the crack growth kinetics as a dual mechanism involving creep by GB sliding and environmental degradation due to dynamic embrittlement by oxygen diffusion.
- GB sliding is only observed if the slip band spacing (SBS) is equal to or larger than a critical limit. An analytical model has been developed to correlate SBS and loading frequency on the basis of minimum strain energy accumulation within slip bands. Results of the model show that a saturation of SBS is reached at approximately 3 microns which is shown to coincide with the transitional loading frequency of 0.01 Hz. GB sliding has been measured from surfaces of intergranular crack growth test specimens using a pre-test scribing method and is estimated to be in the range of 1 to 6 microns.
- An intergranular crack growth model has been developed based on a mechanism involving GB sliding. The model simulates GB cracking process by adapting a CZ approach in which the GB is set as an interface element governed by a linear traction-displacement relationship. The element displacement is calculated as the difference of the total displacement imparted by the surrounding continuum and the viscoplastic strain due to the GB sliding. The continuum deformation is described by a multi-scale model which includes the coupling of a XP model simulating the near crack tip region and a macroscopic ISV model for the far field response several grains removed from the crack tip.
- The accelerated damage in the crack tip GB path in air environment is considered to be a result of GB dynamic embrittlement by oxygen diffusion, the effect of which is to reduce the GB immobility leading ultimately to a localized boundary decohesion. A grain boundary fracture criterion has been formulated in terms of the critical sliding strain in vacuum reduced by a mobility parameter which is a function of the oxygen concentration.
- The CZ model has been applied to simulate the crack tip element's deformation and fracture as a function of loading conditions and environment. Results of this simulation show the crack growth rates for temperatures ranging from 650 to 800°C in both vacuum and air have been predicted and results are in agreement with the range and trends of the experimental data.
- Results of the developed CZ model have been examined in terms of the influence of partial pressure of oxygen and GB viscosity. They show that the crack growth rate is enhanced by the oxygen diffusion and the influence of environment is relatively higher as the temperature decreases. Furthermore, the increase in GB viscosity, which is a function of grain boundary diffusivity and grain boundary modulus, is beneficial to the crack growth resistance.

Acknowledgements

The authors acknowledge the support from the MAI (Metals Affordability Initiative) program, in collaboration with the Air Force Research Lab, Pratt & Whitney, GE Aviation, Georgia Institute of Technology and Ohio State University.

References

1. H. Ghonem, T. Nicholas, and A. Pineau, "Elevated Temperature Fatigue Crack Growth in Alloy 718 – Part I: Effects of Mechanical Variables," *Fatigue and Fracture of Engineering Materials and Structures*, 5 (1993) 565-576.

2. H. Ghonem, T. Nicholas, and A. Pineau, "Elevated Temperature Fatigue Crack Growth in Alloy 718 – Part II: Effects

of Environmental and Material Variables," *Fatigue and Fracture of Engineering Materials and Structures*, 16 (1993) 577-590.
3. H. Ghonem and D. Zheng, "Frequency Interaction in High Temperature Fatigue Crack Growth in Superalloys," *Metallurgical and Materials Transactions A*, 23 (1992) 3067-3072.
4. H. Ghonem and K. Maciejewski, "Mechanistic Modeling of Dwell Fatigue Crack Growth in P/M Nickel-Based Superalloys using a Cohesive Zone Approach," (Report, Metals Affordability Initiative Program, AFRL, 2012).
5. J. Dahal, "Grain Boundary Deformation and Damage Mechanisms in Intergranular Crack Growth of a Nickel Based Superalloy" (Master's thesis, University of Rhode Island, 2011).
6. S. Kirchhoff, "Effects of Microstructure and Environment on Intergranular Crack Growth Behavior of a Powder Metallurgy Nickel Based Superalloy," (Master's thesis, University of Rhode Island, 2008).
7. J. Li, "The Mechanics and Physics of Defect Nucleation," *MRS Bulletin*, 32 (2007) 151-159.
8. M.M. Hall Jr., "Thermally Activated Dislocation Creep Model for Primary Water Stress Cracking of NiCrFe Alloys," (Paper A-I-09, Proceedings of the International Symposium on Plant Aging and Life Prediction of Corrodible Structures, Sapporo, Japan, May, 1995).
9. M.J. Starink and P.A.S Reed, "Thermal Activation of Fatigue Crack Growth: Analysing the Mechanisms of Fatigue Crack Propagation in Superalloys," *Material Science Engineering A*, 491 (2008) 279-289.
10. F.W. Crossman and M.F. Ashby, "The Non-uniform Flow of Polycrystals by Grain Boundary Sliding Accommodated by Power-law Creep," *Acta Metallurgica*, 23 (1975) 425-440.
11. T. Kê, "Experimental Evidence of the Viscous Behavior of Grain Boundaries in Metals," *Physical Review*, 71 (8) (1947) 533-546.
12. F. Cosandey, "Grain Boundary Internal Friction and Relationship to Intergranular Fracture," *Journal De Physique*, C5 (10) (1988) 581-586.
13. E. Arzt, M.F. Ashby, and R.A. Verrall, "Interface Controlled Diffusional Creep," *Acta Metallurgica*, 31 (12) (1983) 1977-1989.
14. H.J. Frost and M.F. Ashby, *Deformation Mechanism Maps: the Plasticity and Creep of Metals and Ceramics* (Oxford, UK: Pergamon Press, 1982).
15. Gell, M., Leverent, G.R., "Mechanisms of High Temperature Fatigue," *Fatigue at Elevated Temperature*, (1973) 37-66.
16. G. Venkataraman, Y.W. Chung, and T. Mura, "Application of Minimum Energy Formalism in a Multiple Slip Band Model for Fatigue I - Calculation of Slip Band Spacing," *Acta Metallurgica*, 39 (1991) 2621-2629.
17. D. Kuhlmaan-Wilsdorf, "Theory of Plastic Deformation: Properties of Low Energy Dislocation Structures, in Low-Energy Dislocation Structures II," 2nd International Conference on Low Energy Dislocation Structures, ed. M.N. Bassim, W.A. Jesser, D. Kuhlmann-Wilsdorf, G.J. Shiflet, *Material Science and Engineering*, (1989) 1-41.
18. A.D. Sheikh-Ali, "On the Influence of Intragranular Slip on Grain Boundary Sliding in Bicrystals," *Scripta Metallurgical et Materialia*, 33 (5) (1995) 795-801.
19. H. Yoshida, K. Yokoyama, N .Shibata, Y. Ikuhara, and T. Sakuma, "High Temperature Grain Boundary Sliding Behaviour and Grain Boundary Energy in Cubic Zirconia Bicrystals," *Acta Metallurgical*, 52 (2004) 2349-57.
20. G.R. Kegg, C.A.P. Horton, and J.M. Silcock, "Grain Boundary Dislocations in Aluminum Bicrystals after High Temperature Deformation," *Philosophical Magazine*, 27 (1973) 1041-1055.
21. R.Z. Valiev, V.G. Khairullin, and A.D. Sheikh-Ali, "Phenomenology and Mechanisms of Grain Boundary Sliding," *Russian Physics Journal*, 34 (3) (1991) 253-261.
22. K. Reading and D. Smith, "A Dynamic Lattice Dislocation Grain Boundary Sliding Mechanism," *Philosophical Magazine A*, 51 (1985) 71-78.
23. P.F. Browning, "Time Dependent Crack Tip Phenomena in Gas Turbine disk Alloys" (PhD thesis, Rensselaer Polytechnic Institute, 1998).
24. A.S. Talekar, "Oxidation Behavior of Nickel Base Superalloys and High Strength Low Alloy Steels at Elevated Temperatures" (PhD thesis, University of Nevada, 2008).